Journal of Molecular Catalysis A: Chemical 295 (2008) 34–38

Contents lists available at ScienceDirect

Journal of Molecular Catalysis A: Chemical

journal homepage: www.elsevier.com/locate/molcata

A novel titanium-supported Ag/Ti electrode for the electro-oxidation of hydrazine

Qingfeng Yi*, Lei Li, Wenqiang Yu, Zhihua Zhou, Guorong Xu

School of chemistry and Chemical Engineering, Hunan University of Science and Technology, Xiangtan 411201, Hunan, China

ARTICLE INFO

Article history:
Received 10 June 2008
Received in revised form 15 August 2008
Accepted 15 August 2008
Available online 30 August 2008

Keywords:
Hydrazine oxidation
Silver electrode
Hydrothermal method
Nanoparticles
Ti electrode

ABSTRACT

Silver nanoparticles were directly deposited on the surface of titanium by the hydrothermal method using polyethylene glycol as the reduction agent. The electrocatalytic activity of the prepared titanium-supported nanoAg/Ti electrode towards hydrazine oxidation in alkaline solutions was evaluated using cyclic voltammetry (CV) and chronoamperometry (CA). The CV results show that the nanoAg/Ti electrode is electrochemically active towards hydrazine oxidation with oxidation potentials ranging between −0.6 and 0.6 V vs. SCE. The onset potential of ca. −0.6 V vs. SCE for the hydrazine oxidation was recorded. A sharp increment in the current density of hydrazine oxidation with the increase of the hydrazine concentration was observed. CA results show stable steady-state current densities (i_{ss}) for the hydrazine oxidation. For the anodic potential holding at 0.1 V, the CA measurement delivered the i_{ss} value of over 0.58 mA cm^{-2} mM^{-1} in the presence of 20 mM hydrazine. A linear dependence of the i_{ss} upon the hydrazine concentration was found in the range of 0–60 mM hydrazine. Results imply that the nanoAg/Ti electrode presents stable and significantly high electroactivity for the hydrazine oxidation.

1. Introduction

Considerable attention has been given to direct liquid fuel cells, such as the methanol, formic acid, hydrazine, and borohydride systems because of their high energy capacity compared to advanced batteries [1]. For the direct hydrazine fuel cell, its most attractive feature may be the high theoretical cell voltage of 1.57 V according to the anode reaction (1) and cathode reaction (2) in alkaline solutions:

$$N_2H_4 + 4OH^- \rightarrow N_2(g) + 4H_2O + 4e E^0 = -1.16\,V vs.SHE \quad (1)$$

$$O_2 + 2H_2O + 4e \rightarrow 4OH^- E^0 = 0.41\,V vs.SHE \quad (2)$$

Thus, there have been increasing reports for the investigation of hydrazine oxidation at various electrocatalysts [2–12]. Hydrazine oxidation on single-crystal platinum surfaces (1 1 1) and (3 2 2) were studied by Alvarez-Ruiz et al. [13,14]. The onset potential of hydrazine oxidation on polyoriented Pt disc electrode in alkaline solutions is ca. 0.1 V vs. SHE (or −0.141 V vs. SCE) [15], showing that the electrochemical oxidation of hydrazine at Pt electrode requires a higher over-potential. O'Mullane et al. have prepared polyaniline (PANI) thin films modified with platinum nanoparticles and investigated their electroactivity for hydrazine oxidation [16]. The electrochemical oxidation of hydrazine at a silver electrode was studied by Korinek et al. [17]. Recently, Gao and co-workers reported the fabrication of Ag nanoparticles on carbon nanotubes (Ag/CNT) and functional multi-walled carbon nanotube surfaces (Ag/MWNT), and evaluated their electroactivity for hydrazine oxidation [18,19]. An onset potential of ca. −0.3 V vs. SCE for the hydrazine oxidation was observed at Ag/MWNT in 0.1 M K_2SO_4 [18]. Electro-oxidation of hydrazine at gold [17,20], nickel [21] and mercury [17,22] electrodes has also been studied. Razmi-Nerbin prepared the nickel pentacyanonitrosylferrate film modified aluminum electrode and evaluated its electroactivity for hydrazine oxidation [23]. Because of a large over-potential for hydrazine oxidation at ordinary carbon electrodes, electrocatalytic modified electrodes based on a variety of catalysts including metals, polymer films and metal complexes were used to minimize the over-potential effects [24]. Cobalt(II) and cobalt(III) complexes have been applied as mediators to modify carbon paste electrodes in order to obtain a catalytic activity for hydrazine oxidation [20,24–26]. In addition, Zare reported the immobilization of rutin at the surface of a glassy carbon electrode (GCE) modified with multi-wall carbon nanotubes (MWCNT), and investigated its electrochemical behavior as a hydrazine sensor [27]. Electrocatalytic activity of catechin film electrochemically deposited on a glassy carbon electrode toward the oxidation of hydrazine was also studied by Zare and Habibirad [28]. Ferreira et al. fabricated a carbon paste electrode by immobilizing Meldola's Blue (MLB) dye on silica–titania phosphate and studied its electroactivity for the hydrazine oxidation [29]. A modified carbon paste electrode prepared by using tetracyanoquinodimethanide adsorbed on silica modified with titanium

* Corresponding author.
E-mail address: yqfyy2001@yahoo.com.cn (Q. Yi).

1381-1169/$ – see front matter © 2008 Elsevier B.V. All rights reserved.
doi:10.1016/j.molcata.2008.08.013

oxide showed an excellent catalytic activity and stability for hydrazine oxidation [30].

In the present study, we have fabricated a novel titanium-supported nano-scale sized silver catalyst (nanoAg/Ti) using a hydrothermal process with a view to obtain a high electrocatalytic effect for hydrazine oxidation. Our recent work showed that titanium is a stable substrate and nano-sized metal particles including nickel [31], binary Pt–Ir [32] and Pt–Ru [33] can be stably immobilized on the Ti surface through the hydrothermal process. The electrochemical activity of the prepared nanoAg/Ti electrode for hydrazine oxidation was assessed using voltammetric techniques and amperometric measurements.

2. Experimental

2.1. Chemicals

Sodium hydroxide (96%), hydrazine hydrate (80%), silver nitrate, polyethylene glycol (EG, MW: 400 g/mol) and other chemicals used in this work were purchased from Sinopharm Group Chemical Reagent Co. Ltd. They were used as received without further purifications. Water (18.2 MΩ cm) used in this work was firstly treated by ion exchange resins and then doubly distilled. Titanium pieces are of 99.2% purity.

2.2. Synthesis and characterization of the nanoAg/Ti

The nanoAg/Ti electrode was fabricated in the following manner. Firstly, the pieces of Ti sheets with the thickness of 1.5 mm were washed with pure water (18.2 MΩ cm), then etched in an 18% HCl solution at 85 °C for 10 min in order to remove the oxides on their surfaces. After that, the sheets were washed with pure water again and subsequently subjected to ultrasonic treatment for 5 min. The pretreated Ti sheets were then transferred in a Teflon container lined autoclave containing 10 mL of 15 mM $AgNO_3$ and 0.5 mL of EG. Then, the container was heated at 120 °C for 12 h. After cooling to room temperature, the coated Ti sheets were removed from the Holder and dried at 100 °C for 30 min.

The morphological texture of the Ag nanoparticles on the Ti surface was studied using scanning electron microscopy (SEM) and energy disperse spectroscopy (EDS) taken on a JSM-6380LV scanning electron microscopy.

2.3. Electrochemical measurements

All electrochemical measurements were performed in Auto-Lab PGSTAT30/FRA (Netherlands) electrochemical instrument. The working electrode was the sample (nanoAg/Ti). The counter electrode was a large Pt foil. Saturated calomel electrode (SCE) was used as the reference electrode positioned as close to the working electrode surface as possible by means of a Luggin capillary. All potentials reported in this paper were against the SCE. The geometric surface area of the sample is 0.2 cm^2. Before experiments, pure nitrogen gas (99.99%) was bubbled through the solution to remove the dissolved oxygen in the solution. During measurements, N_2 was continuously flushed over the surface of the solution. All experiments were carried out at ambient temperature (20 ± 2 °C).

3. Results and discussion

3.1. Morphological characterization of the nanoAg/Ti

Scan electron microscopic (SEM) images of the nanoAg/Ti at different magnifications are shown in Fig. 1. SEM image of Fig. 1a shows a good coverage of catalyst particles on the surface of Ti substrate. The catalyst particles with the sizes of ca. 400–500 nm are connected with each other to form a three-dimensional texture (Fig. 1b). This porous structure provides stable immobilization of the silver particles on the Ti surface. Further analysis of the sample was done by energy dispersive x-ray spectrometry (EDS) shown in Fig. 1(c). Energy peaks at 2.5, 3.0 and 3.15 keV are ascribed to characteristic peaks of silver. The energy peaks at 0.3 and 0.51 keV are assigned to the presence of carbon and oxygen, respectively. This leads to the shadow areas in the SEM image of the nanoAg/Ti.

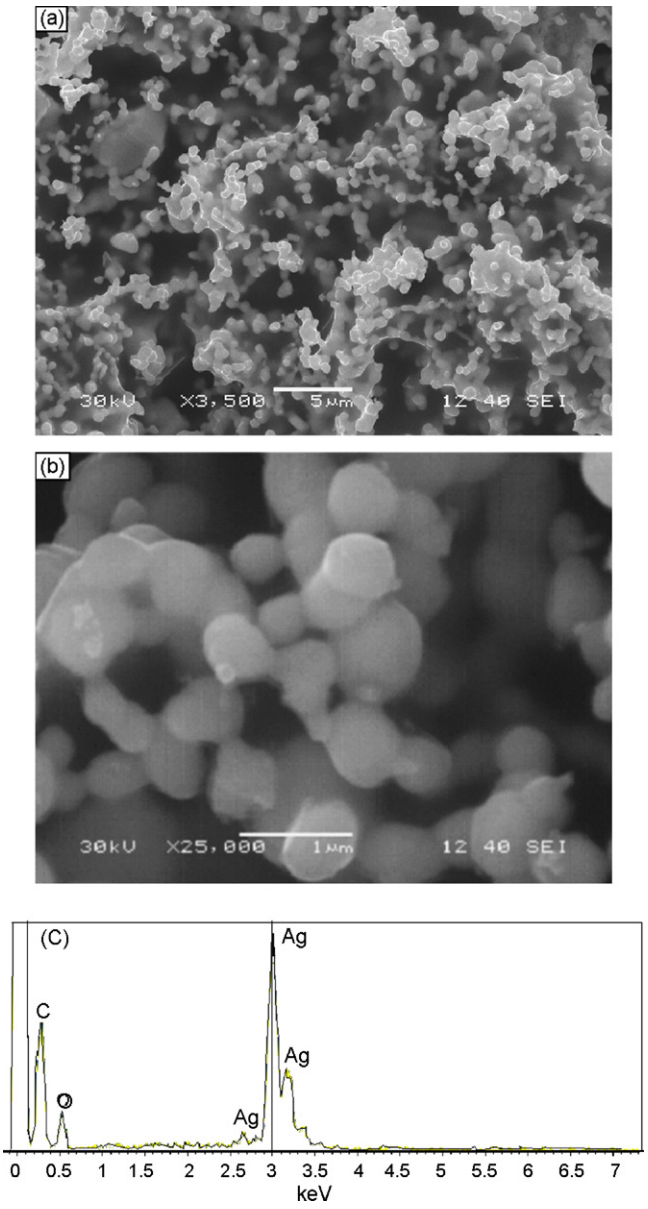

Fig. 1. Scanning electron microscopic (SEM) images of the nanoAg/Ti electrode with different magnifications (a and b) and its energy dispersive spectrometry (EDS).

3.2. Cyclic voltammetric (CV) measurements of nanoAg/Ti

Fig. 2 shows repeatedly scanning CV profiles of the nanoAg/Ti in 1 M NaOH solution in the absence of hydrazine. It is found from Fig. 2 that the nanoAg/Ti presents similar CV profiles to polycrystalline silver electrode except that the nanoAg/Ti exhibits much higher anodic and cathodic current densities than silver electrode

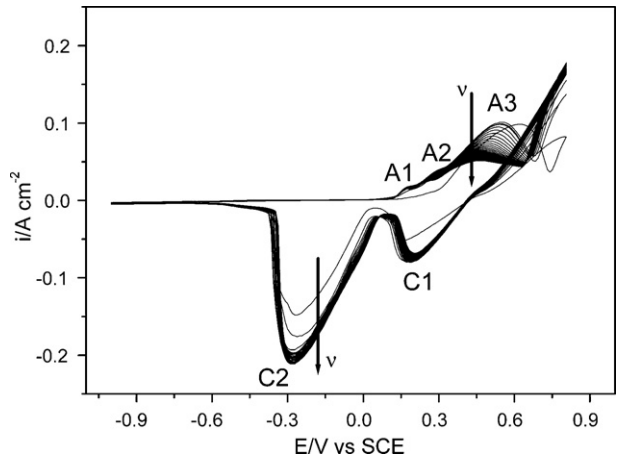

Fig. 2. 50 continuously sweeping cyclic voltammograms of the nanoAg/Ti electrode at a scan rate of 100 mV/s in the 1 M NaOH solution.

[34], showing a large surface area of the nanoAg/Ti electrode. Overlapped CV curves were observed with the increase of cycling numbers, showing highly stable catalyst particles on the Ti surface. In the anodic oxidation range of silver two anodic peaks A1 at ca. 0.170 V and A2 at ca. 0.289 V were registered as shown in Fig. 2. According to Droog et al. [34], the peaks A1 and A2 could be ascribed to the formation of Ag_2O. Among them, the peak A1 is attributed to the production of monolayer Ag_2O. The peaks A1 and A2 is caused by the following reaction:

$$2Ag + 2OH^- = Ag_2O + H_2O + 2e \quad (3)$$

The further forward potential sweep leads to the arising of the peak A3 at 0.43–0.55 V which is attributed to the formation of high-valence silver oxide (AgO):

$$Ag_2O + 2OH^- = 2AgO + H_2O + 2e \quad (4)$$

The variation in the potential of the peak A3 with the cyclic scan number could be related to the unstability of the high-valence AgO. In the reverse scan two reduction peaks C1 and C2 were delivered at ca. 0.19 and −0.28 V, which correspond to the reduction of AgO and Ag_2O, respectively [34]. The high reduction current density in Fig. 2 indicates the presence of large active sites on the surface of the nanoAg/Ti electrode.

Cyclic voltammetric responses of the nanoAg/Ti electrode in 1.0 M NaOH solution containing different hydrazine concentrations are presented in Fig. 3. As seen in Fig. 3a–i, upon the addition of hydrazine, an enhancement in the anodic current density was observed while the cathodic current density decreased. From the

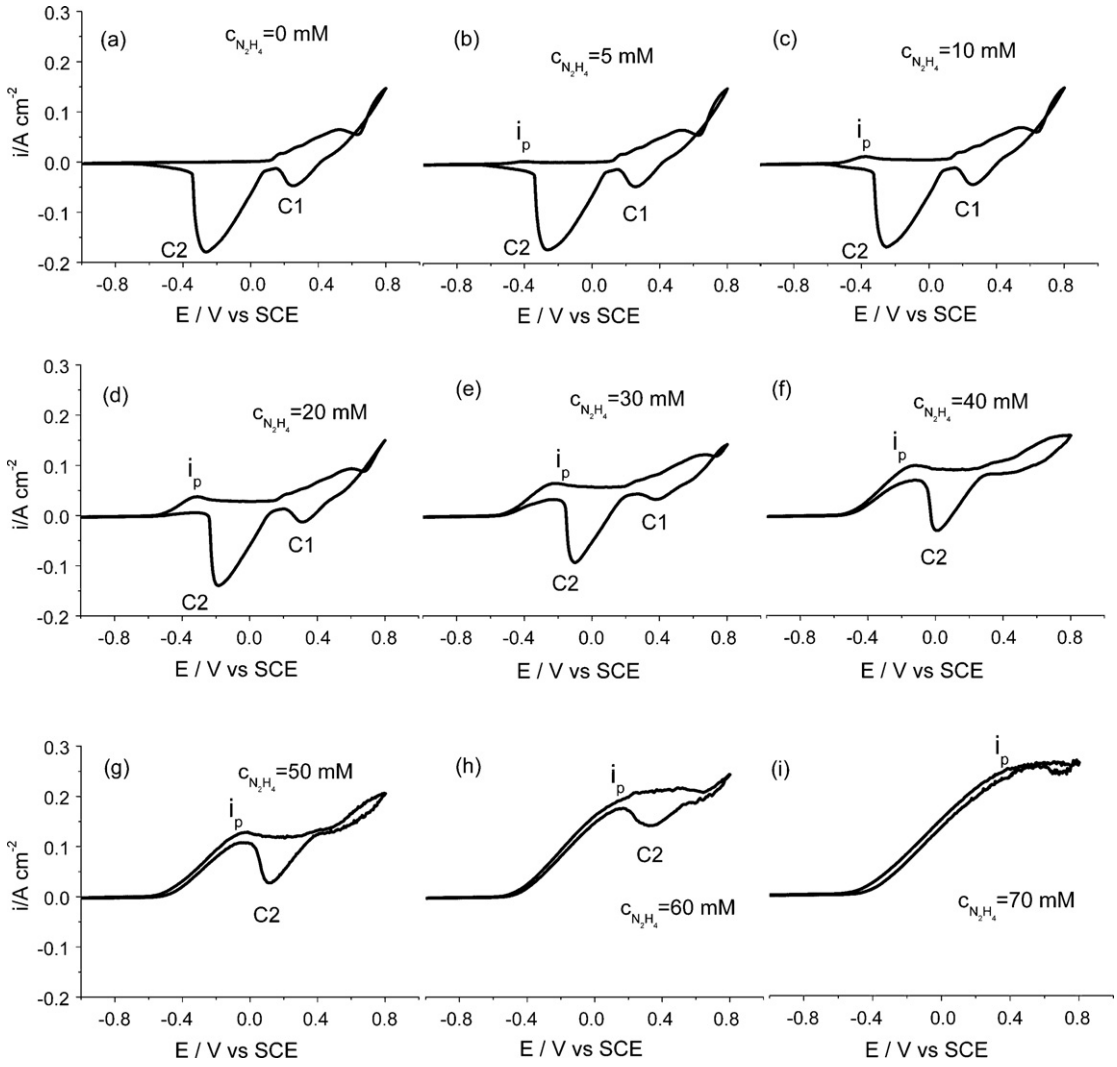

Fig. 3. Cyclic voltammetric responses of the nanoAg/Ti electrode at a scan rate of 100 mV/s in the presence of different hydrazine concentrations in 1 M NaOH solution.

CV profile in the absence of hydrazine (Fig. 3a) and those in the presence of hydrazine (Figs. 3b–i), it is found that an enhancement in the anodic current density commences at the potential of ca. −0.60 V, showing the direct oxidation of hydrazine in the nanoAg/Ti as shown in reaction (1). This is consistent with the observation in the absence of hydrazine shown in Fig. 3a where no anodic electrode reaction was observed in the potential range of −1.0 to 0.1 V. With the increase of hydrazine concentration, the current density for the hydrazine oxidation increases. Conversely, the current densities for the reduction peaks C1 and C2 decrease with the rise in hydrazine concentration. The peak C1 totally disappears in the presence of 40 mM N_2H_4 and the peak C2 also becomes weaker and finally fads away with the hydrazine concentration, indicating that the anodic oxidation of silver particles is inhibited due to the presence of hydrazine. These results show that the prepared nanoAg/Ti electrode presents high electroactivity towards the hydrazine oxidation. At the hydrazine concentration of 70 mM (Fig. 3i) high anodic current density in the backward scan was observed and the reverse scan profile was almost the same as the positive scan one. This could be related to the further oxidation of considerable amount of intermediates formed during the forward scan. The current density for the hydrazine oxidation on the nanoAg/Ti is much higher than those on Ag nanoparticles supported on CNTs [18,19]. It is further observed from Fig. 3 that with the addition of hydrazine, there was an increase in the anodic peak current density. Plot of the anodic peak current density (i_p) vs. added hydrazine concentrations are shown in Fig. 4 where a well linear relationship appears from 0.0 to 50 mM, showing sensitive hydrazine detection at the nanoAg/Ti electrode. Two linear segments with different slopes in Fig. 4 corresponds to two different ranges of hydrazine concentration and could be ascribed to a change in the catalytic reaction conditions due to the formation of nitrogen gas bubbles at the surface of the nanoAg/Ti. At low concentrations of hydrazine, the N_2 gas formed is negligible and has no effect on the diffusion of hydrazine towards the electrode surface. At high concentrations of hydrazine, however, gas evolution is, to some extent, equivalent to stirring solution, enhancing the diffusion of hydrazine towards the electrode surface.

Cyclic voltammograms of a solution containing 20 mM hydrazine in 1.0 M NaOH using the nanoAg/Ti electrode scanned at different scan rates are shown in Fig. 5a. It is found from Fig. 5 that both the anodic and cathodic current densities increase with the scan rates except for the current density of the reduction peak C1. The potential (E_p) of the anodic peak A2 shifts to more positive with the scan rate as shown in Fig. 5b. This result shows that the over-

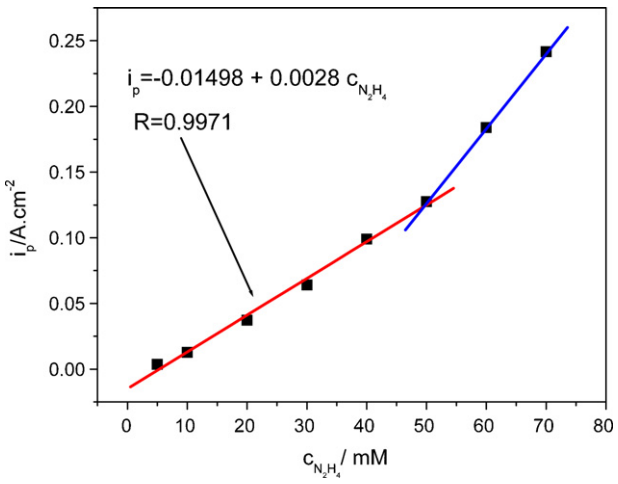

Fig. 4. Plot of the anodic peak current density i_p shown in Fig. 3 vs. hydrazine concentration.

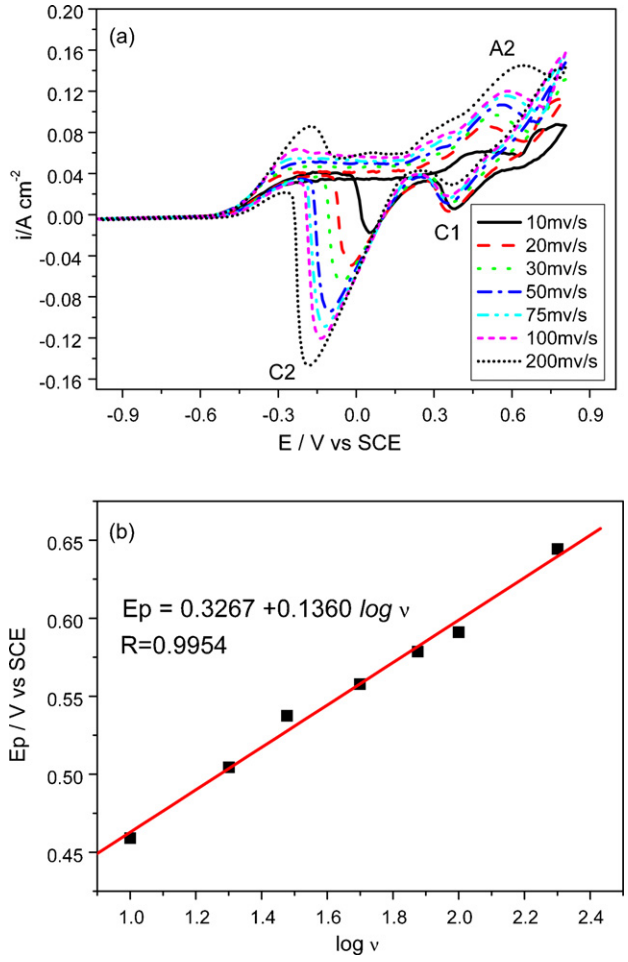

Fig. 5. Cyclic voltammograms (a) for the nanoAg/Ti in 1 M NaOH + 20 mM N_2H_4 solution at potential sweep rates of 10, 20, 30, 50, 75, 100, and 200 mV/s. (b) Relationship of the potential (E_p) of the anodic peak A2 with the logarithm of scan rate.

potential for the generation of high-valence AgO increases with the increase of the scan rate, causing the decrease of the current density of the reduction peak C1 with the scan rate.

3.3. Chronoamperometric data of the nanoAg/Ti

Fig. 6 presents current density–time plots for hydrazine oxidation at the nanoAg/Ti electrode in 1.0 M NaOH + 20 mM N_2H_4 upon different potential steps. At the applied potentials of −0.5, −0.4, −0.3 and 0.1 V, steady-state current densities were observed without pronounced decay of the current density, indicating the high stability of the nanoAg/Ti electrode for the electro-oxidation of hydrazine. The values of current density depend on the potential step, as shown in Fig. 6 where the current density increases with the potential. At t = 300 s, the current densities at potentials of −0.5, −0.4, −0.3 and 0.1 V are 1.21×10^{-4}, 0.24×10^{-2}, 0.715×10^{-2} and 1.15×10^{-2} A cm^{-2}, respectively.

Effect of the hydrazine concentration on chronoamperograms for the nanoAg/Ti electrode at a potential step of 0.10 V is shown in Fig. 7. With the addition of hydrazine, there is an increase in the anodic current density. At $C(N_2H_4)$ = 60 mM, the steady-state current density (i_{ss}) at 300 s is 0.029 A cm^{-2}, showing a larger oxidation rate of hydrazine on the nanoAg/Ti electrode. This results in the visible evolution of N_2 gas on the surface of the nanoAg/Ti. Therefore, the current oscillation at 60 mM hydrazine could be ascribed to the bubbling of N_2 gas through the reaction (2). Fig. 8 shows the plot

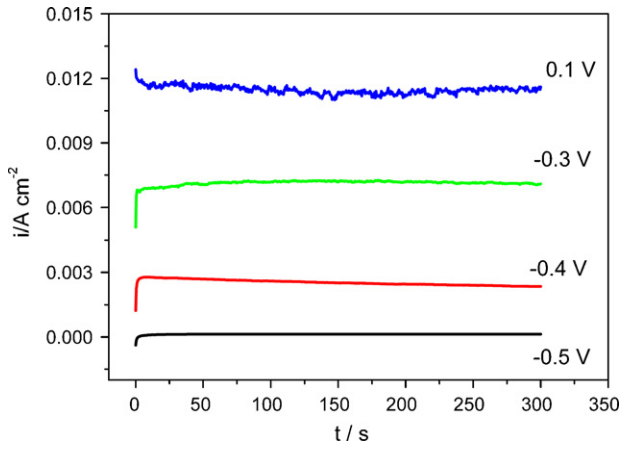

Fig. 6. Chronoamperometric responses for the nanoAg/Ti electrode in the 1 M NaOH + 20 mM N_2H_4 solution at potential steps of −0.5, −0.4, −0.3 and 0.1 V.

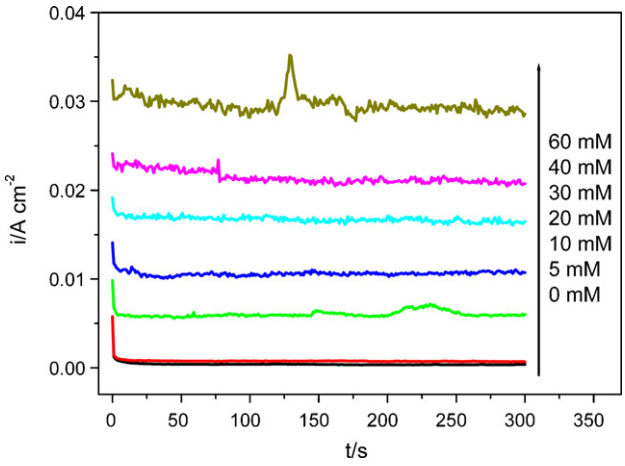

Fig. 7. Chronoamperometric responses for the nanoAg/Ti electrode at the potential step of 0.1 V in 1 M NaOH solution with various hydrazine concentrations.

of current density (i_{ss}) at 300 s as a function of hydrazine concentration. The linear relationship of i_{ss} with $C(N_2H_4)$ reveals that the prepared nanoAg/Ti electrode would be a promising sensor for the detection of hydrazine.

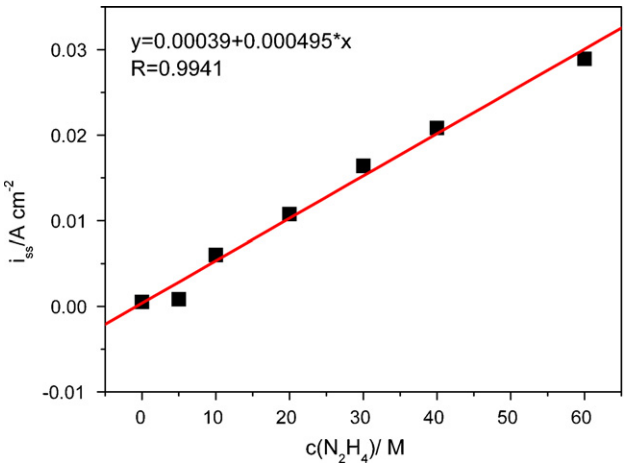

Fig. 8. Dependence of the steady-state current density i_{ss} shown in Fig. 7 upon the hydrazine concentration.

4. Conclusions

Titanium-supported silver nanoparticles (nanoAg/Ti) prepared using the hydrothermal method kept highly electrochemical stability in alkaline solutions. This could be ascribed to the porous network texture of the Ag particles immobilized on the Ti surface. The nanoAg/Ti electrode presented large current density and low onset potential for the hydrazine oxidation. Stable and high steady-state current densities were observed from chronoamperometric measurements at different potential steps and hydrazine concentrations. The high electroactivity of the nanoAg/Ti could be related to its large surface area. Results show that the prepared nanoAg/Ti could be applied to direct hydrazine fuel cells as a potential anodic electrode.

Acknowledgements

This work is supported by the National Natural Science Foundation of China (No. 20876038) and A Project Supported by Scientific Research Fund of Hunan Provincial Education Department, China (07A019). Qingfeng Yi thanks the Project Sponsored by the Scientific Research Foundation for Returned Overseas Chinese Scholars, State Education Ministry, China ([2007]1108).

References

[1] M.H. Atwan, D.O. Northwood, E.L. Gyenge, Int. J. Hydrogen Energy 32 (2007) 3116–3125.
[2] A. Salimi, L. Miranzadeh, R. Hallaj, Talanta 75 (2008) 147–156.
[3] J.B. Zheng, Q.L. Sheng, L. Li, Y. Shen, J. Electroanal. Chem. 611 (2007) 155–161.
[4] K. Yamada, K. Yasuda, H. Tanaka, Y. Miyazaki, T. Kobayashi, J. Power Sources 122 (2003) 132–137.
[5] J. Li, X.Q. Lin, Sens. Actuator B 126 (2007) 527–535.
[6] W.C. Ye, B. Yang, G.Y. Cao, L.Y. Duan, C.M. Wang, Thin Solid Films 516 (2008) 2957–2961.
[7] H.R. Zare, N. Nasirizadeh, Electrochim. Acta 52 (2007) 4153–4160.
[8] K. Yamada, K. Asazawa, K. Yasuda, T. Ioroi, H. Tanaka, Y. Miyazaki, T. Kobayashi, J. Power Sources 115 (2003) 236–242.
[9] A. Salimi, R. Hallaj, Electroanalysis 16 (2004) 1964–1971.
[10] A. Salimi, K. Abdi, Talanta 63 (2004) 475–483.
[11] J.S. Pinter, K.L. Brown, P.A. DeYoung, G.F. Peaslee, Talanta 71 (2007) 1219–1225.
[12] C. Batchelor-McAuley, C.E. Banks, A.O. Simm, T.G.J. Jones, R.G. Compton, Analyst 131 (2006) 106–110.
[13] B. Alvarez-Ruiz, R. Gomez, J.M. Orts, J.M. Feliu, J. Electrochem. Soc. 149 (2002) D35–D45.
[14] C. Nishihara, I.A. Raspini, H. Kondoh, H. Shindo, M. Kaise, H. Nozoye, J. Electroanal. Chem. 338 (1992) 299–315.
[15] V. Rosca, M.T.M. Koper, Electrochim. Acta 53 (2008) 5199–5205.
[16] A.P. O'Mullane, S.E. Dale, T.M. Day, N.R. Wilson, J.V. Macpherson, P.R. Unwin, J. Solid State Electrochem. 10 (2006) 792–807.
[17] K. Korinek, J. Korita, M. Nusiloua, J. Electroanal. Chem. 21 (1969) 421–427.
[18] G.Y. Gao, D.J. Guo, C. Wang, H.L. Li, Electrochem. Commun. 9 (2007) 1582–1586.
[19] G.W. Yang, G.Y. Gao, C. Wang, C.L. Xu, H.L. Li, Carbon 46 (2008) 747–752.
[20] S.M. Golabi, F. Noor-Mohammadi, J. Solid State Electrochem. 2 (1998) 30–37.
[21] M. Felischmann, K. Korinek, D. Plrtcher, J. Electroanal. Chem. 34 (1972) 499–506.
[22] U. Eissner, E. Gileadi, J. Electroanal. Chem. 28 (1970) 81–88.
[23] H. Razmi-Nerbin, M.H. Pournaghi-Azar, J. Solid State Electrochem. 6 (2002) 126–133.
[24] G. Cepriaa, J.R. Castillo, J. Appl. Electrochem. 28 (1998) 65–70.
[25] J.J. Zhang, W.J. Pietro, A.B.P. Lever, J. Electroanal. Chem. 403 (1996) 93–100.
[26] D.W. Pang, H.B. Deng, Z.L. Wang, Electrochim. Acta 39 (1994) 847–854.
[27] H.R. Zare, Z. Sobhani, M. Mazloum-Ardakani, J. Solid State Electrochem. 11 (2007) 971–979.
[28] H.R. Zare, A.M. Habibirad, J. Solid State Electrochem. 10 (2006) 348–359.
[29] C.U. Ferreira, Y. Gushikem, L.T. Kubota, J. Solid State Electrochem. 4 (2000) 298–303.
[30] J.C. Duarte, R. de Cássia Silva Luz, F.S. Damos, A.B. de Oliveira, L.T. Kubota, J. Solid State Electrochem. 11 (2007) 631–638.
[31] Q.F. Yi, W. Huang, J.J. Zhang, X.P. Liu, L. Li, J. Electroanal. Chem. 610 (2007) 163–170.
[32] Q.F. Yi, A. Chen, W. Huang, J.J. Zhang, X.P. Liu, G.R. Xu, Z.H. Zhou, Electrochem. Commun. 9 (2007) 1513–1518.
[33] K. Koczkur, Q.F. Yi, A. Chen, Adv. Mater. 19 (2007) 2648–2652.
[34] J.M.M. Droog, P.T. Alderliesten, G.A. Bootsma, J. Electroanal. Chem. 99 (1979) 173–186.